Available online at www.sciencedirect.com
ScienceDirect
Applied Catalysis A: General 332 (2007) 8–21
APPLIED CATALYSIS A: GENERAL
www.elsevier.com/locate/apcata

Mathematical modeling and simulation of hydrotreating reactors: Cocurrent versus countercurrent operations

Fabián S. Mederos [a], Jorge Ancheyta [a,b,*]

[a] *Instituto Mexicano del Petróleo, Eje Central Lázaro Cárdenas 152, Col. San Bartolo Atepehuacan, México D.F. 07730, México*
[b] *ESIQIE-IPN, UPALM, México D.F. 07738, México*

Received 23 March 2007; received in revised form 17 July 2007; accepted 21 July 2007
Available online 31 July 2007

Abstract

This paper describes a model to predict the behavior of trickle-bed reactors used for catalytic hydrotreating of oil fractions with cocurrent and countercurrent operation modes. A dynamic plug-flow heterogeneous one-dimensional model, which has been previously validated with experimental data obtained in an isothermal pilot plant reactor with cocurrent operation, was employed to compare both modes of operation. The reactor model considers the main reactions present in the hydrotreating process: hydrodesulfurization, hydrodenitrogenation, and hydrodearomatization. Simulations were performed for both pilot and commercial trickle-bed reactors, and the results are discussed in terms of variations with time and axial position of partial pressure, temperature and concentrations in liquid phase. A superior performance of countercurrent operation mode was found over cocurrent mode. It was recognized that countercurrent mode can have great potential to be used for deep hydrodesulfurization of oil fractions since it minimizes the inhibiting effect of some products (e.g. H_2S) in reactor zones where these species tend to concentrate in cocurrent operation, i.e. at the bottom of the catalytic bed.

Keywords: Modeling; Hydrotreating; Cocurrent; Countercurrent

1. Introduction

Since various years ago refiners have been subject to continuous pressure to produce the so-called ultra-low sulfur diesel. This pressure will continue in the near future due to new and more severe specifications in sulfur content (15 wppm since 2006 in the US and 10 wppm around 2008 in the EU) [1–4]. Catalytic hydrotreatment (HDT), a mature technology with proven commercial experience, has been extensively used to achieve the current fuels quality, however, in order to fulfill the even more stringent environmental requirements it is necessary to have a deep understanding on the behavior of the HDT process from different points of view: catalyst formulation, process configuration, reactor design, feed selection, reactor internals, effect of operating conditions, combination with other emerging technologies, etc.

It has been recognized that the achievement of almost zero values of sulfur in fuels has to be done through a combination of more than one of these approaches. The study of some of them depends totally or partially on experimental work, e.g. catalyst formulation, feed selection, however others (process configuration, operating conditions, reactor design, etc.) can be undertaken theoretically via process modeling and simulation. Being the three-phase catalytic reactor the heart of an HDT unit, this equipment is then the target for modeling purposes. In HDT reactors gas and liquid phases (hydrogen and hydrocarbons) are contacted with a solid phase (catalyst). The reactions occur between the dissolved gas reactant and the liquid-phase reactant at the surface of the catalyst.

Depending on whether the main mass-transfer resistance is located, three-phase catalytic fixed-bed reactors are operated either with a continuous gas and a distributed liquid phase (trickle operation), or with a distributed gas and a continuous liquid phase (bubble operation). Commercial HDT processes usually operate in a trickle-bed regime, with cocurrent downward flow of gas and liquid over a randomly fixed bed of catalyst particles while reactions take place [5–8].

It is well known that sulfur removal is strongly inhibited by the competitive adsorption effect of H_2S at the sulfided active sites of the catalyst. According to different authors [9–11], even

* Corresponding author. Fax: +52 55 9175 8429.
E-mail address: jancheyt@imp.mx (J. Ancheyta).

0926-860X/$ – see front matter
doi:10.1016/j.apcata.2007.07.028

Nomenclature

a	dimensionless number of Glaso's correlation
a_j	specific surface area at the interface j (cm^{-1})
A	aromatic compound
API	API gravity
B	saturated hydrocarbon
c_{pj}	specific heat capacity of j phase ($J\ g^{-1}\ K^{-1}$)
C_i^j	molar concentration of compound i in the j phase ($mol\ cm^{-3}$)
d_{pe}	equivalent particle diameter (cm)
d_{15}	liquid density at 15 °C ($g\ cm^{-3}$)
$d_{15.6}$	specific gravity at 15.6 °C
D_i^j	molecular diffusivity of compound i in the j phase ($cm^2\ s^{-1}$)
D_a^L	axial mass dispersion coefficient in the liquid phase ($cm^2\ s^{-1}$)
E_a	activation energy ($J\ mol^{-1}$)
Ga_L	Gallileo number of liquid phase
G_L	liquid superficial mass velocity ($g\ cm^{-2}\ s^{-1}$)
h_{GL}	heat-transfer coefficient for gas–liquid interface ($J\ s^{-1}\ cm^{-2}\ K^{-1}$)
h_{LS}	heat-transfer coefficient for liquid film surrounding the catalyst particle ($J\ s^{-1}\ cm^{-2}\ K^{-1}$)
H_i	Henry's law constant for compound i ($MPa\ cm^3\ mol^{-1}$)
ΔH_{ads}	adsorption enthalpy of H_2S ($J\ mol^{-1}$)
ΔH_{Rj}	heat of reaction j ($J\ mol^{-1}$)
HDA	hydrodearomatization reaction
HDN	hydrodenitrogenation reaction
HDS	hydrodesulfurization reaction
j_H	j factor for heat transfer
k_f	forward HDA rate constant ($s^{-1}\ MPa^{-1}$)
k_j	apparent j (= HDS, HDN_B, and HDN_{NB}) reaction rate constant, see Table 1
k_L	thermal conductivity of liquid phase ($J\ s^{-1}\ cm^{-1}\ K^{-1}$)
k_r	reverse HDA rate constant (s^{-1})
k_0	frequency factor, see Table 1
k_i^j	mass-transfer coefficient of compound i at the interface j ($cm\ s^{-1}$)
K_{H_2S}	adsorption equilibrium constant for H_2S ($cm^3\ mol^{-1}$)
L_B	length of catalyst bed (cm)
p_i^j	partial pressure of compound i in the j phase (MPa)
P	reactor total pressure (psia)
$Pe_{a,m}^L$	Peclet number for axial mass dispersion in liquid phase
r_j	reaction rate j ($mol\ cm^{-3}\ s^{-1}$, for j = HDS $mol\ g^{-3}\ s^{-1}$)
R	universal gas constant ($J\ mol^{-1}\ K^{-1}$)
Re_j	Reynolds number of j phase
t	time (s)
T_j	temperature of j phase (K)
T_{MeABP}	mean average boiling point (°R)
u_j	superficial velocity of j phase ($cm\ s^{-1}$)
z	axial coordinate (cm)

Greek letters

$\Delta\rho_T$	temperature correction of liquid density ($lb\ ft^{-3}$)
$\Delta\rho_P$	pressure dependence of liquid density ($lb\ ft^{-3}$)
$\in$	bed void fraction
ε_j	holdup of j phase
ε_p	particle porosity
η_j	catalyst effectiveness factor for reaction j
λ_i	solubility coefficient of the compound i ($Nl\ kg^{-1}\ MPa^{-1}$)
ρ_B	catalyst bulk density ($g\ cm^{-3}$)
ρ_j	density at process conditions of j phase ($lb\ ft^{-3}$)
ρ_0	liquid density at standard conditions (15.6 °C; 101.3 kPa) ($lb\ ft^{-3}$)
ρ_{20}	liquid density at 20 °C ($g\ cm^{-3}$)
μ_L	absolute viscosity of the liquid (mPa s)
v_c	critical specific volume of the gaseous compounds ($cm^3\ mol^{-1}$)
v_i	molar volume of solute i at its normal boiling temperature ($cm^3\ mol^{-1}$)
v_L	molar volume of solvent liquid at its normal boiling temperature ($cm^3\ mol^{-1}$)
v_N	molar gas volume at standard conditions ($Nl\ mol^{-1}$)
v_C^m	critical specific volume ($ft^3\ lb_m^{-1}$)
ζ	fractional volume of the catalyst bed diluted by inert particles

Subscripts

0	reactor inlet condition
A	aromatics
G	gas phase
HC	desulfurized or denitrogeneted hydrocarbon
H_2	hydrogen
H_2S	hydrogen sulfide
j	reaction (HDS, HDN_B, HDN_{NB}, or HDA)
L	liquid phase or gas–liquid interface
N_B	basic nitrogen
N_{NB}	nonbasic nitrogen
NH_3	ammonia
S	organic sulfur compound, solid phase or liquid–solid interface

Superscripts

G	gas phase
L	liquid phase or gas–liquid interface
S	solid phase or liquid–solid interface

low increases of H_2S at the entrance of the reactor can substantially reduce hydrodesulfurization (HDS) reaction rate. It is therefore mandatory to maintain the reaction under H_2S concentration as low as possible by efficient removal of the H_2S produced during the reaction. For trickle-bed operation cocurrent downward flow has unfavorable hydrogen and

hydrogen sulfide concentration profiles over the reactor, i.e. high H_2S concentration at the reactor outlet [12]. A more suitable profile of H_2S concentration can be provided by operating the reactor in countercurrent mode, for instance, introducing the feed at the top and H_2 at the bottom of the reactor, as proposed by Trambouze [13].

Countercurrent operation can be considered as an advanced technology, which has been patented by ABB Lummus Crest Inc. and commercialized in 1971 as the Lummus Arosat process for hydrogenation of aromatics [14], which is enhanced by lower temperature and higher hydrogen partial pressure both obtained in countercurrent operation [15,16]. It has been reported recently that the Lummus Arosat hydrogenation process could produce ultra-clean diesel with 1 wppm sulfur and 4 vol% aromatic contents [17].

Despite its technical importance in order to achieve deep HDS, it should be noted that detailed reaction engineering studies of countercurrent operation of HDT reactors are limited. Most of the research for HDT process is about the conventional cocurrent trickle-bed reactor (TBR) [1,18–26], while only a few papers concerning the analysis of countercurrent TBRs have been reported [13,27–31]. Modeling of countercurrent operation has been demonstrated to be complicated because of the partial evaporation of the light liquid feedstocks, which involves detailed local thermodynamic equilibrium calculations along the reactor (compositions in gas and liquid phases, interfacial temperatures, latent heats of vaporization, etc.), increasing considerably the computing time and risk to fail in reaching the accurate solution of the model [23,27].

The main objective of this work is to extend the research for developing advanced clean fuel technology by evaluating the performance of the countercurrent TBR in comparison with the typical cocurrent downflow TBR under similar reaction conditions. Variations of liquid and gas velocities and the effect of H_2S partial pressure are illustrated. The advantages and disadvantages of cocurrent and countercurrent modes of operation are also addressed. Detailed optimization and economic feasibility are beyond the scope of this paper.

2. Cocurrent and countercurrent operation modes

To effectively do the catalyst and reactor selection and process development, a good knowledge of what various reactor types can and cannot do is critical [32]. Therefore, in this section the similarities and differences between TBRs with cocurrent downward flow and countercurrent gas–liquid flow (Fig. 1) are outlined.

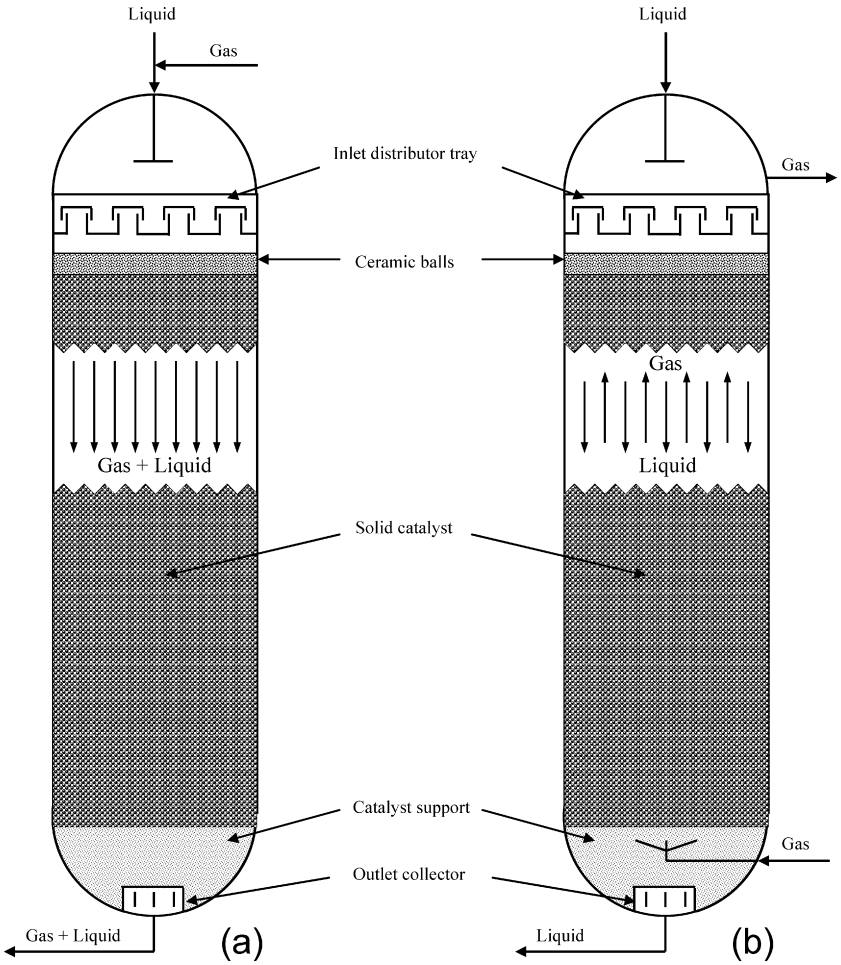

Fig. 1. Schematic diagrams of catalytic fixed-bed reactors: (a) trickle-bed with cocurrent downward flow, (b) trickle-bed with countercurrent flow.

2.1. Selection of flow direction

The three-phase catalytic reactors are recognized as reactors of choice when, from a reaction engineering perspective, a large catalyst to liquid volume ratio is desired (a plug-flow of both phases is preferred in this case), reaction rates are not excessively high, and catalyst deactivation is very slow or negligible. Once a three-phase catalytic reactor with fixed bed has been chosen as a reactor for conversion of gas and liquid reactants, the frequently asked question is whether to use an upflow, downflow or countercurrent flow modes of operation [32].

The selection of the direction of liquid and gas flows can be dictated according to the chemical system design, such as equilibrium limitations, throughput limitations by flooding, pressure drop, required degree of conversion, heat recovery, availability of driving forces for mass transfer and chemical reaction [33,34], or as was pointed out by Dudukovic et al. [32], the choice of upflow versus downflow reactors can be based on rational considerations as to where the limiting reactant at the operating conditions of interest is. In accordance to this, if the limiting reactant is a liquid-phase compound present in low concentration, as it would be for the case of HDS of a feedstock containing small amounts of organo-sulfur compounds, the choice will be upflow operation because it provides complete catalyst wetting and the fastest mass transport of the liquid reactant to the solid particle. On the other hand, for gas-limited reactions a downflow reactor is preferred as it favors the mass transport of the gaseous reactant to the catalyst. However, it has been also demonstrated that when the bed is packed with inert fines material, the differences between upflow and downflow disappear completely since mass transport effects in both modes of operation come to be identical.

Goto and Smith [35] have shown that cocurrent operation is preferred for conversion to desirable products and high gas rates. For gas purification, countercurrent operation is preferable as long as the liquid feed contains none of the gaseous impurity. They also concluded that the differences between cocurrent and countercurrent flows are not large except for plug-flow conditions.

According to Iliuta et al. [36] the countercurrent mode of operation is usually adopted when larger mean concentration driving forces are needed. However, when an irreversible reaction occurs (like hydrodearomatization), there is no difference in the mean concentration driving force in the two modes of operation.

2.2. Conventional TBR with cocurrent gas–liquid downflow

The most frequently used TBR for HDT of oil fractions is that with cocurrent downward flow of gas and liquid. A TBR consists of a column that can be very high (above 10–30 m) equipped with a fixed bed of solid catalyst packing, throughout which gas and liquid reactants flow cocurrently downward [37].

The liquid and gas flow rates are very low in such a level that the liquid tickles over the packing forming a laminar film, drops or rivulets, and the gas flows continuously through the voids in the bed [38]. This flow pattern is termed the trickle flow (gas continuous region or homogeneous flow) and is the type of flow usually obtained in laboratory- and pilot-scale reactors, although, some researchers establish that this flow pattern is much closer to plug-flow. On the other hand, for the higher operating flow rates of gas and/or liquid in commercial reactors the flow pattern is described as rippling, slugging or pulsing flow [6]. Cocurrent downward operation mode is the most used in practice because it has less severe limitations in throughput than in cocurrent upflow and countercurrent operations [33].

Even when completely vapor-phase reaction in a fixed catalyst bed may be technically feasible, a TBR may be preferred for the saving in energy costs associated with reactant vaporization (i.e. HDS of naphtha). The limiting reactant may be essentially all in the liquid phase or in both liquid and gas phases, and the distribution of reactants and products between gas and liquid phases may vary with conversion [6].

A TBR is also used for absorption of the gas into a reacting liquid, when the ratio of the liquid to the gas flow rate is either very low or very high [36]. It has been shown that for a bench-scale TBR the liquid velocity and the catalyst bed length have important effects on the performance of the reactor [5]. Low liquid flow rate causes partial wetting of the catalyst and consequently a decrease in conversion of the limiting reactant. However, this phenomenon of partial wetting may have positive effects on the reaction rate when gas–liquid mass transfer is the major rate limitation. Nevertheless it reduces selectivity as far as consecutive reactions are concerned [39].

The main advantages and disadvantages of TBR with cocurrent downflow are the following. It will be further deduced that the advantages justify the extensive use of cocurrent downflow TBR to improve both the conversion degree (productivity) and increase the yield of the desired product (selectivity) [37].

Advantages:

- Low catalyst loss [6,10,20,37,40–44].
- Low pressure drop [6,36,38,45].
- Easy design [37,46].
- No moving parts [20,37].
- Low investment and operating costs [7,37,41,43,44].
- Operation at high pressures and temperatures in a safe way [20,37,44].
- Minimum occurrence of homogeneous side-reactions [6,37,40,42,44].
- Wide range of throughput demands [20,32,36,37,43,45].
- Liquid flow approaching ideal plug-flow behavior which leads to high conversions [7,8,20,37,40,42–44].
- No limitations arise from the phenomenon of flooding [36,40,43–45,47].
- Gas flow improves liquid distribution [40], and does not affect mass-transfer resistances [47].
- Recommended for gas-limited reactions [32].

Disadvantages:

- Low catalyst effectiveness [10,37].
- Limitations with viscous or foaming liquids [37].
- Incomplete catalyst wetting [6,7,8,32,37–39,41].
- Sensitivity to thermal effects [37,39,44].
- Low liquid holdup [32].
- High inhibiting effect by H_2S in HDS of refractory sulfur compounds [6,8,27].
- High suppression of activity of the hydrocracking catalyst and inhibition of the HDN reaction by NH_3 [6,8,27].
- Cementation because of soft or deformable catalyst [6].
- Plugging of bed by fouling products [37].
- Deactivation of catalyst by deposits [6,7,37].
- Dismantling of the reactor during catalyst replacement [42,44].
- Low conversions in equilibrium limited reactions [27].
- Bypassing of liquid by wall flow [6].
- Limited to reasonably fast reactions [42,43].

2.3. TBRs with countercurrent gas–liquid flow (or submerged upflow reactors)

Because a catalytic TBR with countercurrent mode has a very large catalytic surface area to reactor volume ratio it is a suitable alternative to HDT [8]. The introduction of TBRs with countercurrent flow in a number of refining operations is likely either via re-design of existing reactors or as new technology. As mentioned earlier, the goal of this mode of operation is not an improvement in reactant mass transfer, which is not rate limiting, but enhanced selective removal of by-products that may act as inhibitors (like H_2S and NH_3) for certain HDT reactions or *in situ* product separation. The differences between co- and countercurrent flows become more pronounced for stronger H_2S inhibition, higher liquid rates, and plug-flow conditions.

Due to the need for removal of the most refractory sulfur compounds in diesel HDS, in which H_2S inhibition effect plays a very important role, countercurrent flow operation mode will become more prominent in the future for processes that suffer from by-product catalyst inhibition [27,32,35,47].

The main problem with countercurrent operation mode in a TBR is the phenomenon of flooding, although it can be undertaken by shaping the catalyst or arranging the packing in order to create different paths for gas and liquid, reducing momentum transfer between the two phases and thereby shifting the flooding limits to much higher flow rates [27].

In the case of hydroprocessing the major disadvantage of countercurrent reactor for commercial applications is due to hardware limitations. The catalyst loading is 20–25% by volume in countercurrent operation (though less catalyst volume is necessary for the countercurrent operation for achieving the same conversion), whereas in cocurrent TBR, the catalyst loading is 60–70% by volume. There is, therefore, a need to develop improved hardware configurations that allow countercurrent contacting of gas and liquid in the presence of small size catalyst particles and also when the catalyst loading is above 50% by volume [8].

The countercurrent mode of operation would be much more desirable for deep HDS processes since this reaction is strongly inhibited by the H_2S produced during sulfur removal. Hydrodesulfurization of oil fractions follows reaction order higher than one with respect to sulfur content, due to the presence of large number of sulfur compounds with different reactivities. The most reactive sulfur compounds are removed in the first part of the reactor while the less reactive sulfur compounds are eliminated in the final part of the reactor. Therefore, countercurrent is the most favorable mode of operation at those conditions because the larger part of the reactor operates under H_2S lean regime, being H_2S concentration the lowest at the bottom of the reactor, and the partial pressure of H_2 at the outlet section of the reactor is the highest. Countercurrent TBRs have reported a reduction in catalyst volume of about 15–20% for HDT of gas oils compared with cocurrent operation for the same conversion level [31,34,46].

For other processes different to HDT, countercurrent operation is used in cases where a diluted feed of highly soluble gas is used as a reactant or in gas-removal processes where a significant conversion of gas-phase reactant is the objective [42].

From this analysis one can conclude that in addition to the design parameters of feed rates and compositions, catalyst particle size, catalyst loading, and intrinsic rate can have a pronounced effect on reactor performance. Therefore, the preferred three-phase reactor for one reaction will not necessarily be the optimum for a different reaction [47].

The advantages and disadvantages of TBR with countercurrent flow are:

Advantages:

- Low partial pressure of H_2S and NH_3 in large part of the catalytic bed [8,13,27,32,46].
- Improved conversions normally limited by chemical equilibrium [8,13,27,32,46].
- Favored with respect to large heat of reaction [8].
- Enables handling more difficult feedstocks to obtain higher conversion [8,27,32,46].
- More favorable flat axial temperature profile [8].
- Large surface area for vapor–liquid mass transfer [8].
- High ratio of active sites to reactor volume [8,27,46].
- Easy catalyst handling [8].
- Significant performance for high liquid rates [47].
- Decreased intraparticle resistance by using small particles [47].
- Adapted when larger mean concentration driving forces are needed [36].

Disadvantages:

- Excessive pressure drop at high liquid and gas velocities [8,27,31–34,36].
- Presence of flooding at high liquid throughputs [8,13,27,31–34,36].
- Lack of correlations to estimate hydrodynamics, mass- and heat-transfer parameters [32].

- Extra constraints to catalyst packing, mainly about its size and shape [13,27,31,34].
- Reduced gas–liquid mass transfer [27].
- Less effective temperature control because of gas flow [27].
- Lack of flexibility with respect to the flow rate of the fluid phases [13].
- Low solid to reactor volume ratio [13,33].
- Low gas–liquid interfacial area [13,33].
- High axial dispersion effects in the liquid phase [48].

3. Modeling of cocurrent and countercurrent TBR operations

3.1. Reactor model

As it was indicated in the previous section, when subproducts (e.g. H_2S) inhibit the reaction (e.g. HDS), the countercurrent operation is expected to have advantages over the cocurrent operation. Therefore, in this work both operations were simulated using a dynamic TBR reactor model (one-dimensional plug-flow heterogeneous), which was validated elsewhere with experimental information obtained at pilot plant scale for the HDT of vacuum gas oil (VGO) [25]. The model is based on that reported by Korsten and Hoffmann [19], who described the HDS of VGO under isothermal conditions, and by Rodríguez and Ancheyta [24], who modeled hydrodesulfurization, hydrodearomatization and hydrodenitrogenation of VGO under isothermal and adiabatic conditions.

To develop heat and mass balances the following assumptions were considered:

(1) The reactors operate in dynamic regime.
(2) Gas and liquid flows can be either cocurrent or countercurrent.
(3) Gas and liquid velocities are constants through the reactor.
(4) Constant density of gas and liquid phases.
(5) There are not radial concentration and temperature gradients.
(6) Catalyst activity does not change with time.
(7) Vaporization and condensation of oil do not take place.
(8) Constant pressure.
(9) Chemical reactions take place only at the solid catalyst.
(10) Mass resistance in the gas side of the gas–liquid interface is assumed to be negligible.

3.1.1. Mass balance

Mass-balance equations in the TBR for cocurrent and countercurrent operations are described with the following set of partial differential equations (PDEs) and ordinary differential equations (ODEs):

(i) Gas phase

$$\frac{\varepsilon_G}{RT_G}\frac{\partial p_i^G}{\partial t} = \pm\frac{u_G}{RT_G}\frac{\partial p_i^G}{\partial z} - k_i^L a_L\left(\frac{p_i^G}{H_i} - C_i^L\right) \quad (1)$$

where $i = H_2$, H_2S, and NH_3. "−" sign is for cocurrent operation and the "+" sign is for countercurrent operation.

(ii) Liquid phase

$$\varepsilon_L\frac{\partial C_i^L}{\partial t} = -u_L\frac{\partial C_i^L}{\partial z} + k_i^L a_L\left(\frac{p_i^G}{H_i} - C_i^L\right) - k_i^S a_S(C_i^L - C_i^S) \quad (2)$$

where $i = H_2$, H_2S, and NH_3.

$$\varepsilon_L\frac{\partial C_i^L}{\partial t} = -u_L\frac{\partial C_i^L}{\partial z} - k_i^S a_S(C_i^L - C_i^S) \quad (3)$$

where i = S, HC, N_B, N_{NB}, and A.

If axial dispersion in the liquid phase is taken into account, Eqs. (2) and (3) need to be replaced by:

$$\varepsilon_L\frac{\partial C_i^L}{\partial t} = -u_L\frac{\partial C_i^L}{\partial z} + \varepsilon_L D_a^L\frac{\partial^2 C_i^L}{\partial z^2} + k_i^L a_L\left(\frac{p_i^G}{H_i} - C_i^L\right) - k_i^S a_S(C_i^L - C_i^S) \quad (2a)$$

$$\varepsilon_L\frac{\partial C_i^L}{\partial t} = -u_L\frac{\partial C_i^L}{\partial z} + \varepsilon_L D_a^L\frac{\partial^2 C_i^L}{\partial z^2} - k_i^S a_S(C_i^L - C_i^S) \quad (3a)$$

In these equations, axial dispersion coefficient of liquid phase (D_a^L) is needed, which can be determined from the Peclet number:

$$Pe_{a,m}^L = \frac{d_{pe}u_L}{D_a^L\varepsilon_L} \quad (4)$$

Peclet number can be calculated from different correlations reported in the literature depending on the mode of operation of the reactor. Some of the reported correlations to account for axial dispersion in the liquid phase are the following:

Cocurrent operation:

1. Sater–Levenspiel correlation for high interaction regime, commercial unit [51].

$$Pe_{a,m}^L = 7.58\times10^{-3}\,Re_L^{0.703} \quad (4a)$$

2. Hochman–Effron correlation for low interaction regime, pilot plant [51].

$$Pe_{a,m}^L = 0.034\,Re_L^{0.5}10^{0.003Re_G} \quad (4b)$$

3. Iliuta correlation for high interaction regime, commercial unit [36].

$$Pe_{a,m}^L = 0.021\,Re_L^{0.97} \quad (4c)$$

4. Iliuta correlation for low interaction regime, pilot plant [36].

$$Pe_{a,m}^L = 0.012\,Re_L^{0.77}10^{0.0011Re_G} \quad (4d)$$

Countercurrent operation:

1. Otake–Kunugita correlation [36].

$$Pe_{a,m}^L = 3.8\,Re_L Ga_L^{-0.33} \quad (4e)$$

2. Sater–Levenspiel correlation [48].

$$Pe^{L}_{a,m} = 7.58 \times 10^{-3}\, Re_L^{0.703} \quad (4f)$$

3. Michell–Furzer correlation [44].

$$Pe^{L}_{a,m} = 1.00(Re_L/\varepsilon_L)^{0.70} Ga_L^{-0.32} \quad (4g)$$

The lack of suitable and reliable correlations to estimate Peclet number and hence axial dispersion coefficient of liquid phase makes it difficult to obtain appropriate estimations, since predictions can vary significantly from one correlation to another. So that, for the purpose of this study we do not consider convenient to report these type of results.

Axial dispersion may influence only the results of small-scale reactors since for commercial reactors it can be neglected. Thus, in our results, if present, axial dispersion is only affecting pilot plant simulations. However, since we are reporting a comparative study of countercurrent versus cocurrent operation, not having the effect of axial dispersion in both modes of operation is not significant and the conclusions will not change. Therefore, the assumption of plug-flow behavior is justified.

(iii) Solid phase

$$\varepsilon_p(1-\in)\frac{\partial C_i^S}{\partial t} = k_i^S a_S (C_i^L - C_i^S) \pm \rho_B \zeta \eta_j r_j(C_i^S, \ldots, T_S) \quad (5)$$

where $i = H_2$, H_2S, NH_3, S, HC, N_B, N_{NB}, and A; j = HDS, HDN_{NB}, HDN_B, and HDA. "−" sign is for the reactants, and the "+" sign is for the products. Reaction rate for ammonia is $r_{NH_3} = -r_{HDN_B} + r_{HDN_{NB}}$.

Because the concentration of hydrocarbon is the main component of the feedstock and it does not change significantly during HDT of VGO, Eqs. (3) and (5) for i = HC will not be considered in the simulations.

3.1.2. Energy balance

To model commercial HDT reactors operating under adiabatic conditions and taking into account that HDT reactions are exothermic in nature, the following energy-balance equations were used:

(i) Gas phase

$$\varepsilon_G \rho_G c_{pG} \frac{\partial T_G}{\partial t} = \pm u_G \rho_G c_{pG} \frac{\partial T_G}{\partial z} - h_{GL} a_L (T_G - T_L) \quad (6)$$

"−" sign is for cocurrent operation and the "+" sign is for countercurrent operation.

(ii) Liquid phase

$$\varepsilon_L \rho_L c_{pL} \frac{\partial T_L}{\partial t} = -u_L \rho_L c_{pL} \frac{\partial T_L}{\partial z} + h_{GL} a_L (T_G - T_L) - h_{LS} a_S (T_L - T_S) \quad (7)$$

(iii) Solid phase

$$(1-\in)\rho_S c_{pS} \frac{\partial T_S}{\partial t} = h_{LS} a_S (T_L - T_S) + \sum_j \rho_B \eta_j r_j (C_i^S, \ldots, T_S)(-\Delta H_R) \quad (8)$$

According to van Hasselt et al. [27] and Ojeda and Krishna [31] for countercurrent operation it is important to include the gas phase in the energy-balance equations to accurately model the heat-transfer process in the reactor because upstream heat transfer from the gas phase to the liquid phase will speed up the reaction rate leading to an even higher concentration of H_2S in the liquid phase at the initial part of the reactor.

3.2. Reaction kinetics, fluid properties and other parameters

The oil fraction feedstock contains a great amount of organic sulfur compounds, and the overall HDS reaction is usually represented by the practical and widely accepted generalized stoichiometric equation, that lumps the HDS reaction of all of the sulfur compounds into one expression.

HDS reaction rate was represented by a kinetic model of Langmuir–Hinshelwood type, where the inhibiting effect of H_2S is taken into account by including an adsorption equilibrium constant of H_2S described by the van't Hoff equation, in order to account for the influence of the temperature in the adsorption of H_2S on the active sites of the catalyst [19]. HDA reaction was modeled by a first-order reversible reaction. HDN was considered as a consecutive reaction in which nonbasic nitrogen compounds are hydrogenated first to basic nitrogen compounds, which undergo further reactions to eliminate the nitrogen atom from the molecule and thus forming ammonia.

HDS, HDA and HDN kinetic models and the corresponding parameters are summarized in Table 1.

The reactor model makes use of correlations taken from the literature to estimate various parameters, such as heat- and mass-transfer coefficients, gas solubilities, and properties of oil and gases under process conditions, which are presented in Table 2 [19,24,25].

Goto and Smith [47] reported that gas flow rates do not have a significant effect on the gas–liquid and liquid–solid mass-transfer coefficients in TBRs, so that the same mass-transfer coefficient values are used for the cocurrent and countercurrent operations permitting so to clarify the kinetic effects [28].

3.3. Model boundary conditions and solution

Since the mathematical model is a system of PDEs and ODEs with time and spatial coordinate as independent variables, it is necessary to define the following initial and

Table 1
Kinetic and thermodynamic data

	Reaction	Kinetic model	E_a (J/mol)	k_0	ΔH_R [d] (J/mol)
HDS	$\upsilon_S S_{(liquid)} + \upsilon_{H_2} H_{2(gas)} \rightarrow \upsilon_{HC} HC_{(liquid)} + \upsilon_{H_2S} H_2S_{(gas)}$	$r_{HDS} = \frac{k_{HDS}(C_S^S)(C_{H_2}^S)^{0.45}}{(1+K_{H_2S}C_{H_2S}^S)^2}$ [a]	131,993	4.266×10^9 cm^3 g^{-1} s^{-1} (cm^3 mol^{-1})$^{0.45}$	−251,000
		$K_{H_2S}(T_S) = k_{0,H_2S}\exp\left(\frac{\Delta H_{ads}}{RT_S}\right)$	2,761[e]	41,770 cm^3 mol^{-1}	
HDN	$N_{NB} \overset{k_{HDN_{NB}}}{\longrightarrow} N_B \overset{k_{HDN_B}}{\longrightarrow} HC + NH_3$				−64,850
Nonbasic		$r_{HDN_{NB}} = k_{HDN_{NB}}(C_{N_{NB}}^S)^{1.5}$ [b]	164,942[f]	3.62×10^6 s^{-1} (wt%)$^{-0.5}$	
Basic		$r_{HDN_B} = k_{HDN_{NB}}(C_{N_{NB}}^S)^{1.5} - k_{HDN_B}(C_{N_B}^S)^{1.5}$	204,341[g]	3.66×10^{11} s^{-1} (wt%)$^{-0.5}$	
HDA	$A \underset{k_r}{\overset{k_f}{\rightleftarrows}} B$	$r_{HDA} = k_f p_{H_2}^G C_A^S - k_r(1 - C_A^S)$ [c]			−255,000
Forward			121,400	1.041×10^5 s^{-1} MPa^{-1}	
Reverse			186,400	8.805×10^9 s^{-1}	

[a] From ref. [19].
[b] From ref. [49].
[c] From ref. [50].
[d] Taken from ref. [51].
[e] ΔH_{ads}.
[f] E_a of $N_{NB} \overset{k_{HDN_{NB}}}{\longrightarrow} N_B$.
[g] E_a of $N_B \overset{k_{HDN_B}}{\longrightarrow} HC + NH_3$.

boundary conditions for the liquid and gas phases and for both modes of operation:

(i) Initial conditions:

For $t = 0$, At $z = 0$,
- Cocurrent operation
  $p_i^G = (p_i^G)_0$, $i = H_2$, H_2S and NH_3
  $C_i^L = (C_i^L)_0$, $i = H_2$, H_2S and NH_3
- Countercurrent operation
  $p_i^G = 0$, $i = H_2$, H_2S and NH_3
  $C_i^L = 0$, $i = H_2$, H_2S and NH_3
- Cocurrent/countercurrent operation
  $C_i^L = (C_i^L)_0$, i = S, N_B, N_{NB}, and A
  $C_i^S = 0$, $i = H_2$, H_2S, NH_3, S, N_B, N_{NB}, and A

$$T_G = T_L = T_S = T_0 \quad (9)$$

At $0 < z < L_B$,
- Cocurrent/countercurrent operation
  $p_i^G = 0$, $i = H_2$, H_2S, and NH_3
  $C_i^L = 0$, $i = H_2$, H_2S, NH_3, S, N_B, N_{NB}, and A
  $C_i^S = 0$, $i = H_2$, H_2S, NH_3, S, N_B, N_{NB}, and A

$$T_G = T_L = T_S = T_0 \quad (10)$$

At $z = L_B$,
- Cocurrent operation
  $p_i^G = 0$, $i = H_2$, H_2S and NH_3
- Countercurrent operation
  $p_i^G = (p_{H_2}^G)_0$, $i = H_2$, H_2S and NH_3
- Cocurrent/countercurrent operation
  $C_i^L = 0$, $i = H_2$, H_2S, NH_3, S, N_B, N_{NB}, and A
  $C_i^S = 0$, $i = H_2$, H_2S, NH_3, S, N_B, N_{NB}, and A

$$T_G = T_L = T_S = T_0 \quad (11)$$

(ii) Boundary conditions:

For $t > 0$, At $z = 0$,
- Cocurrent operation
  $p_i^G = (p_i^G)_0$, $i = H_2$, H_2S and NH_3
  $C_i^L = (C_i^L)_0$, $i = H_2$, H_2S and NH_3
  $T_G = (T_G)_0$
- Countercurrent operation
  $C_i^L = 0$, $i = H_2$, H_2S and NH_3
- Cocurrent/countercurrent operation
  $C_i^L = (C_i^L)_0$, i = S, N_B, N_{NB}, and A
  $C_i^S = 0$, $i = H_2$, H_2S, NH_3, S, N_B, N_{NB}, and A

$$T_L = (T_L)_0;\ T_S = (T_S)_0 \quad (12)$$

At $z = L_B$
- Countercurrent operation
  $p_i^G = (p_i^G)_{L_B}$, $i = H_2$, H_2S and NH_3
  $T_G = (T_G)_{L_B}$
- Cocurrent/countercurrent operation with liquid axial dispersion

$$\frac{\partial C_i^L}{\partial z} = 0 \quad (13)$$

When a high-purity hydrogen stream without gas recycle is used, such as in the case of some laboratory and bench-scale HDT reactors, or when the gas recycle has been subject to purification process in commercial units, values of partial pressures (p_i^G) and liquid molar concentrations (C_i^L) of H_2S and NH_3 at the entrance of the catalytic bed ($z = 0$ and $z = L_B$ for cocurrent and countercurrent operation, respectively) are equal or very close to zero.

The PDEs describing the heat and mass transfer in the reactor were transformed into a set of first-order ODEs by discretization in the axial direction using the backward finite difference method and leaving the independent variable time without discretize. The ODEs with initial conditions were then solved using the fourth-order Runge–Kutta method. This approach is also known as the method of lines. The program required to calculate transport

Table 2
Correlations to estimate heat- and mass-transfer coefficients, gas solubilities and properties of oil and gases [19,24,25]

Parameter	Correlation
Oil density	$\rho_L(P,T_L)=\rho_0+\Delta\rho_P-\Delta\rho_T$
	$\Delta\rho_P=\left[0.167+\left(16.181\times10^{-0.0425\rho_0}\right)\right]\left(\frac{P}{1000}\right)-0.01\left[0.299+\left(263\times10^{-0.0603\rho_0}\right)\right]\left(\frac{P}{1000}\right)^2$
	$\Delta\rho_T=\left[0.0133+152.4(\rho_0+\Delta\rho_P)^{-2.45}\right](T_L-520)-\left[8.1\times10^{-6}-0.0622\times10^{-0.764(\rho_0+\Delta\rho_P)}\right](T_L-520)^2$
Henry coefficient	$H_i=\frac{v_N}{\lambda_i\rho_L}$
Solubility of hydrogen	$\lambda_{H_2}=-0.559729-0.42947\times10^{-3}T_L+3.07539\times10^{-3}\left(\frac{T_L}{\rho_{20}}\right)+1.94593\times10^{-6}T_L^2+\frac{0.835783}{\rho_{20}^2}$
Solubility of H_2S	$\lambda_{H_2S}=\exp(3.367-0.00847\,T_L)$
Gas–liquid mass-transfer coefficient	$\frac{k_i^L a_L}{D_i^L}=7\left(\frac{G_L}{\mu_L}\right)^{0.4}\left(\frac{\mu_L}{\rho_L D_i^L}\right)^{1/2}$
Dynamic liquid viscosity	$\mu_L=3.141\times10^{10}(T_L-460)^{-3.444}[\log_{10}(\mathrm{API})]^a$
	$a=10.313[\log_{10}(T_L-460)]-36.447$
Diffusivity	$D_i^L=8.93\times10^{-8}\left(\frac{v_L^{0.267}}{v_i^{0.433}}\right)\left(\frac{T_L}{\mu_L}\right)$
Molar volume	$v=0.285v_c^{1.048}$
	$v_c^m=7.5214\times10^{-3}T_{MeABP}^{0.2896}\cdot d_{15.6}^{-0.7666}$
Liquid–solid mass-transfer coefficient	$\frac{k_i^S}{D_i^L a_S}=1.8\left(\frac{G_L}{a_S\mu_L}\right)^{1/2}\left(\frac{\mu_L}{\rho_L D_i^L}\right)^{1/3}$
Specific surface area	$a_S=\frac{6}{d_{pe}}(1-\in)$
Liquid–solid heat-transfer coefficient[a]	$j_H=\frac{h_{LS}}{c_{pL}\mu_L\rho_L}\left(\frac{c_{pL}\mu_L}{k_L}\right)^{2/3}$

[a] Taken from ref. [52].

coefficients and to simultaneously solve the system of ODEs was coded in FORTRAN language.

4. Results and discussion

The feedstock and catalyst used for simulation were a VGO and a NiMo/Al_2O_3 commercial sample, which main properties are given in Table 3. Isothermal pilot reactor and adiabatic commercial TBR were simulated under the conditions reported in Table 4.

4.1. Simulation of an isothermal HDT pilot plant

Simulations using the reactor model described in Section 3 were carried out to observe the behavior of the two modes of operation (cocurrent and countercurrent). Since in this case the reactor is operated isothermally, only mass-balance equations were considered.

There are two ways to simulate cocurrent TBR for HDT of oil fractions, one is by considering that the oil is saturated with H_2 at the entrance of the reactor [19], and the other one is by assuming that the oil is not saturated with H_2, that is, the initial H_2 concentration in oil is zero ($(C_{H_2}^L)_0=0$) in Eqs. (9) and (12). This latter approach was used by Yamada and Goto [28] in order to be able to compare cocurrent and countercurrent operation modes under equal initial conditions. Both approaches were modeled in the present work.

Fig. 2 shows how sulfur in the product at the exit of the reactor changes as a function of time for cocurrent operation with VGO saturated and not saturated with H_2 and for countercurrent operation. The dynamic profiles of nitrogen (basic and nonbasic) and total aromatics contents in the product

Table 3
Main properties of HDT feedstock and catalyst

Property	Value
Feedstock	
API gravity	22
Molecular weight	441.9
Mean average boiling point (°C)	476
Sulfur (wt%)	2.009
Total nitrogen (wppm)	1284
Basic nitrogen (wppm)	518
Total aromatics (wt%)	41.9
Catalyst	
Equivalent diameter (mm)	2.54
Specific surface area (m^2/g)	175
Pore volume (cm^3/g)	0.56
Mean pore diameter (Å)	127
Molybdenum content (wt%)	10.7
Nickel content (wt%)	2.9
Bulk density (g/cm^3)	0.8163

Table 4
Operation conditions

	Pilot reactor	Commercial reactor
Gas superficial velocity (cm/s)	0.28	10.27
Oil superficial velocity (cm/s)	1.75×10^{-2}	0.63
Catalytic bed length (cm)	31.58	853.44
Internal diameter (cm)	2.54	304.8
LHSV (h^{-1})	2	2.66
H_2/Oil ratio (scf/Bbl)	2000	2000
Temperature (°C)	380	380
Pressure (MPa)	5.3	5.3
Gas composition (mol%)		
H_2	100	81.63
H_2S	–	3.06
Light hydrocarbons	–	15.31

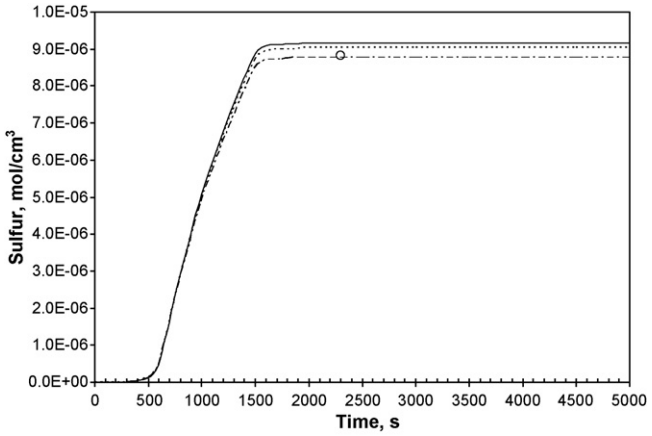

Fig. 2. Concentration of organic sulfur compound at the outlet of the catalytic bed ($z = 31.58$ cm) as function of time (pilot reactor, 380 °C; 5.3 MPa; $u_L = 1.75 \times 10^{-2}$ cm/s; $u_G = 0.28$ cm/s). (▬ · ▬, —, and - - -) simulated, (○) experimental value. (▬ · ▬) cocurrent with H_2 saturated oil, (—) cocurrent with unsaturated oil, (- - -) countercurrent.

at the exit of the reactor exhibited the same trends, which are also similar to those reported elsewhere [25].

The steady state is obtained at about the same time (2300 s) for the three approaches. Before it is reached, the three profiles are almost identical. After 1000 s cocurrent with unsaturated oil yields higher sulfur contents followed by countercurrent and then by cocurrent with H_2 saturated oil operations. It is worthy to mention that cocurrent with H_2 saturated oil is the approach which better reproduces the experimental value because the kinetic parameters were initially optimized with this condition. Similar to sulfur, nitrogen and aromatics follow the same trends for all approaches, i.e. having zero concentration at the exit of the reactor from zero to about 250 s, since at the beginning these compounds are present only in the hydrocarbon feed which flows down through the catalytic bed, and no matter the way of injecting hydrogen their concentrations diminish from the top to the bottom of the reactor.

Fig. 3 presents the steady state liquid molar concentration profiles of sulfur, nonbasic nitrogen, basic nitrogen, and aromatics along the catalytic bed with cocurrent downward flow of gas and liquid (saturated and unsaturated with H_2) and countercurrent operation. We can see from this figure that for all operation modes sulfur content in the liquid phase (and also other impurities content) decreases through the reactor. It is also observed that the lowest sulfur content in the product is obtained for cocurrent operation with the oil saturated with H_2 before it enters to the reactor. This latter performance has been reported previously by Wache et al. [4].

It is also possible to confirm the tendency reported by others, in which concentration of sulfur compounds for cocurrent operation is lower than that of countercurrent operation in about 73% of the reactor length and then the tendency switches [28]. This behavior is because in countercurrent operation the initial part of the reactor (at the top) has high H_2S concentration, whereas around the outlet of the reactor (at the bottom) there is low H_2S concentration, which makes the HDS reaction rate less

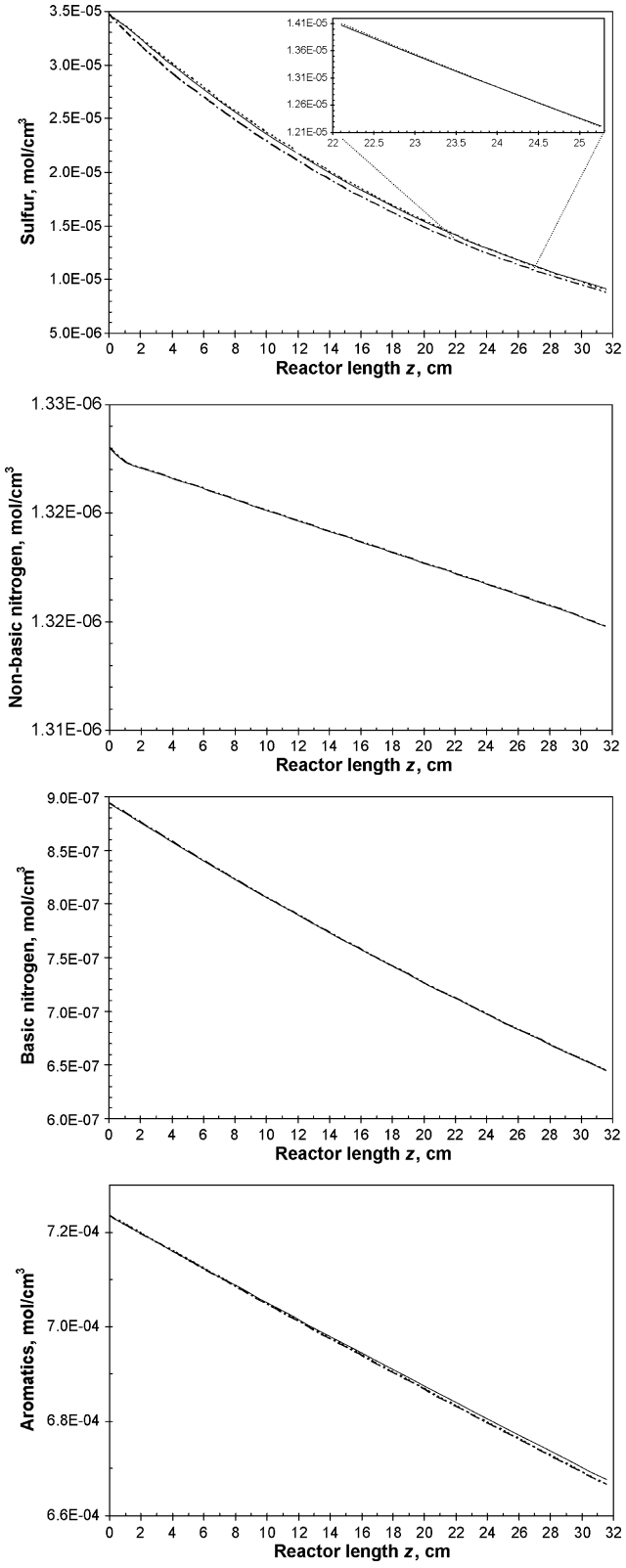

Fig. 3. Sulfur, nonbasic nitrogen, basic nitrogen, and aromatics concentration profiles at steady state down through catalytic bed. (▬ · ▬) Cocurrent with H_2 saturated oil, (—) cocurrent with unsaturated oil, (- - -) countercurrent.

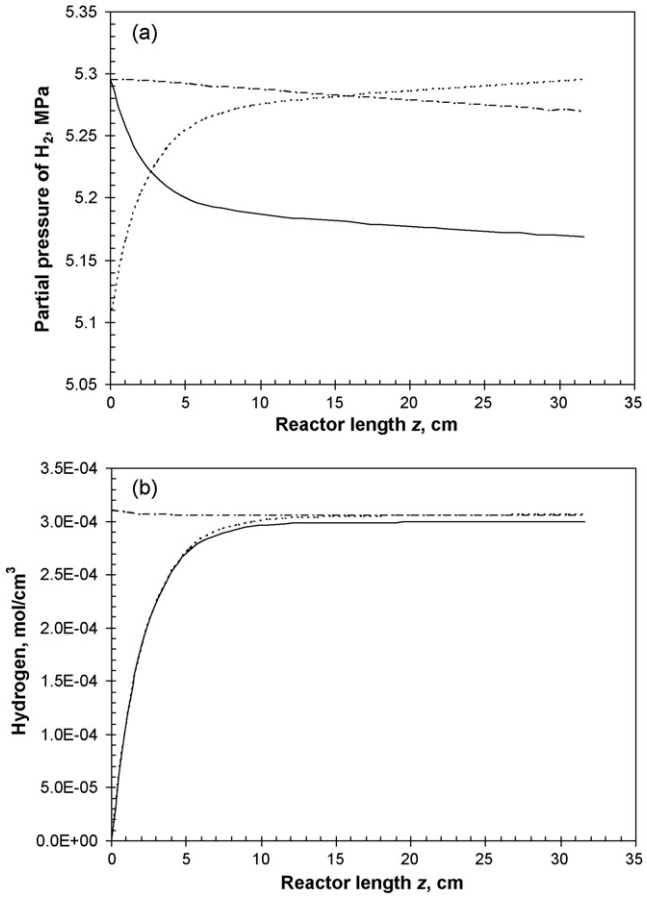

Fig. 4. (a) H_2 partial pressures and (b) H_2 concentration profiles at steady state down through the catalytic bed. (▬ · ▬) Cocurrent with H_2 saturated oil, (—) cocurrent with unsaturated oil, (- - -) countercurrent.

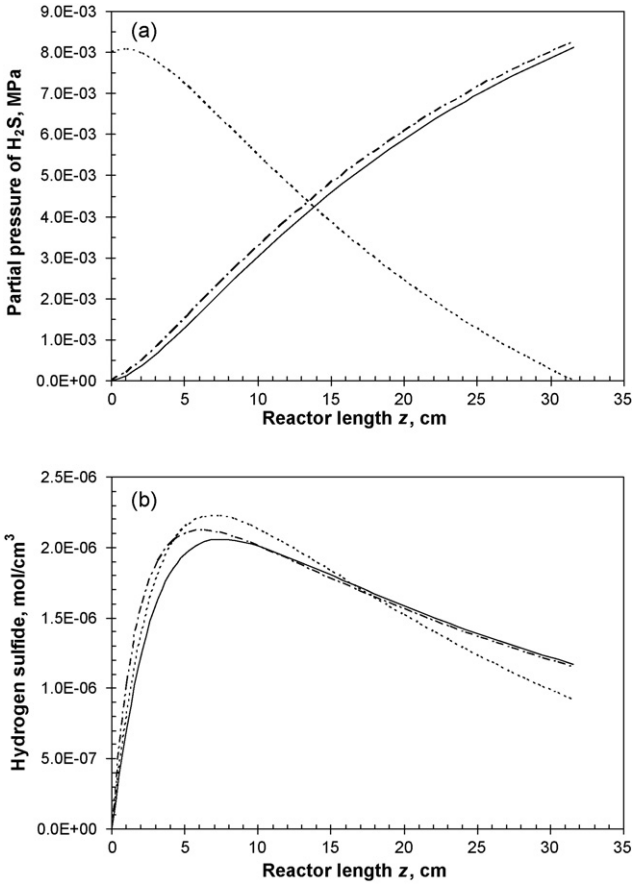

Fig. 5. (a) H_2S partial pressures and (b) H_2S concentration profiles at steady state down through the catalytic bed of pilot plant. (▬ · ▬) Cocurrent with H_2 saturated oil, (—) cocurrent with unsaturated oil; (- - -) countercurrent.

inhibited by H_2S and thus faster than that of the cocurrent operation.

Partial pressure and concentration profiles of H_2 and H_2S along the reactor when the steady state is reached for the three approaches are shown in Figs. 4 and 5, respectively. In all cases the overall shape of molar concentration profiles of H_2 and H_2S are determined by the balance between the reaction rate and mass transfer.

Trends for concentration profiles of H_2S in the liquid phase are similar for the two modes of operation, while for partial pressures profiles of H_2 and H_2S the tendencies are opposite. This opposite pattern is obviously expected since at the top of the reactor ($z = 0$) cocurrent operation has high H_2 content and low H_2S content, while countercurrent operation has low H_2 content and high H_2S content at the top of the reactor.

From Fig. 4 we can see that for cocurrent operation with H_2 saturated oil, the concentration of H_2 in the liquid phase slightly decreases at the beginning of the reactor until certain point because of the high reaction rate in this zone, then it starts to increase by the large mass transfer of H_2 to the liquid phase. While for cocurrent operation with unsaturated oil, the H_2 concentration in the liquid phase increases rapidly due to the high H_2 dissolving rate.

The results presented in Fig. 5 corroborate what is reported in the literature about the H_2S concentration profile in the liquid phase along the reactor [18–21,23–25,27–30]. That is for all operation modes the H_2S concentration in the liquid phase increases and then decreases, and for cocurrent operation partial pressure of H_2S always increases through the catalytic bed, and countercurrent operation exhibits a contrary tendency.

4.2. Simulation of an HDT commercial unit

Once the reactor model was used to simulate the countercurrent operation in the isothermal pilot reactor, it was applied to predict the behavior of a commercial HDT adiabatic reactor in countercurrent operation. For such a case, the energy-balance equations (Eqs. (6)–(8)) were also considered in the simulations along with the mass-balance equations. When comparing cocurrent and countercurrent modes of operation, it was assumed that the heat and mass-transfer coefficients are identical independently of the phase flow direction as proposed by Trambouze [13].

Fig. 6 illustrates the results of dynamic simulation of the commercial reactor. The profiles of sulfur content at the outlet of the catalytic bed for cocurrent operation with VGO saturated and not saturated with H_2 and for countercurrent operation are presented. For the three modes of operation the steady state is reached a little bit faster than that observed for the pilot reactor, which agrees with previous reports [25].

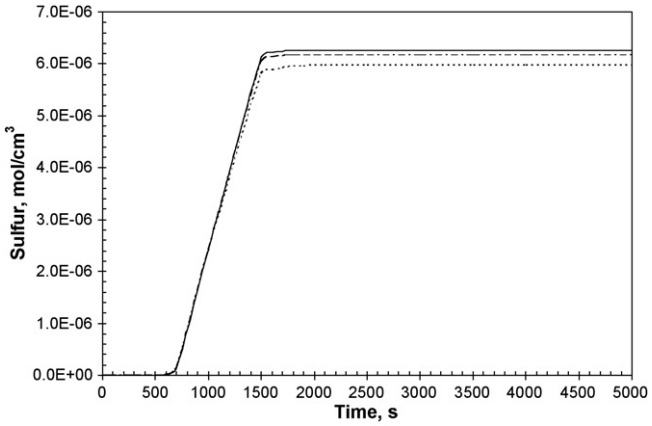

Fig. 6. Concentration of organic sulfur compound at the outlet of the catalytic bed (z = 853.44 cm) as function of time (commercial reactor, 380 °C; 5.3 MPa; u_L = 0.63 cm/s; u_G = 10.27 cm/s). (▬ ▪ ▬) Cocurrent with H_2 saturated oil, (—) cocurrent with unsaturated oil, (- - -) countercurrent.

Contrary to pilot plant operation, in which cocurrent mode with H_2 saturated oil showed the highest impurities removal, in this case countercurrent operation gives the highest conversions. This better performance of countercurrent operation mode can be explained as follows: when the reactants move further down the reactor, mass transfer of H_2S from the liquid to the gas phase prevails and then the liquid H_2S concentration decreases, as was reported by van Hasselt et al. [27] and Ojeda and Krishna [31]. This relatively small difference between the two modes of operation may have a great impact for commercial applications. For instance if a current HDS unit is producing a 500 wppm sulfur diesel, the modification of the actual cocurrent to countercurrent operation would reduce sulfur content.

Fig. 7a shows the dynamic temperature profiles at the exit of the reactor of the liquid phase, and Fig. 7b presents the evolution of temperature of liquid phase along the reactor for both cocurrent and countercurrent operations. The temperature profile of gas phase through the catalytic bed for countercurrent operation is also shown in Fig. 7b. Since the countercurrent operation gave the highest sulfur conversion as was described previously (Fig. 6), the highest liquid temperature at the exit of the reactor would be also expected, however this is not the situation as can be observed in Fig. 7a. The liquid temperature for countercurrent operation resulted to be lower (in a marginal amount, but lower) than that predicted by the cocurrent operation with VGO saturated with H_2. This behavior leads to the conclusion that the ascending gas phase cools the liquid phase along the catalytic bed of the reactor [31].

Fig. 7b confirms this phenomenon at the exit of the reactor, but this only happens at the very end of the reactor. Cooling of liquid phase by gas phase is due to the temperature at which the gas is fed to the reactor.

Fig. 8a and b show the simulation results of partial pressure and concentration of H_2S in the liquid phase respectively for the three modes of operation. As was already reported, conversion of sulfur in commercial scale (adiabatic) is higher than that of pilot scale (isothermal) at similar conditions [25], therefore, the

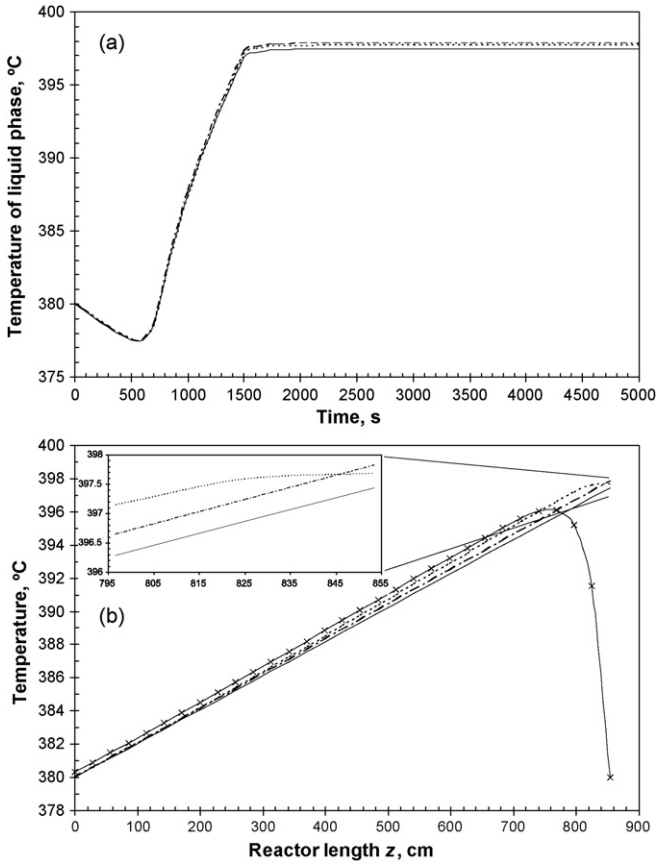

Fig. 7. Temperature profiles: (a) of liquid phase at the outlet of the catalytic bed (z = 853.44 cm) as a function of time, and (b) along the catalytic bed. (▬ ▪ ▬) Cocurrent with H_2 saturated oil, (—) cocurrent with unsaturated oil, (- - -) liquid phase countercurrent, (—×—) gas-phase countercurrent.

H_2S concentration in the liquid phase is larger in commercial reactor and its effect is also greater than that observed at pilot scale. As can be seen in Fig. 8a, the tendencies of partial pressure of H_2S are in general similar to those found at pilot plant (Fig. 5a). Only cocurrent operation with VGO not saturated with H_2 presented a decrease in the partial pressure of H_2S in the initial part of the reactor because the H_2S is rapidly dissolved in the liquid phase until a point where its saturation is reached, and then the mass transfer is changed from the liquid phase to the gas phase. In comparison with the pilot reactor with countercurrent operation, the commercial reactor presents a higher H_2S partial pressure than the cocurrent operation with unsaturated oil beyond the half-part of the reactor due to its improved liquid–gas mass-transfer condition, which is called by some authors as *in situ* stripping of H_2S from the liquid phase [30,31].

The high reaction rate in the initial part (10%) of the catalyst bed provokes a rapid increase in the liquid H_2S concentration for all the modes of operation. The accumulation of H_2S in the liquid phase is more pronounced in cocurrent operation with VGO saturated with H_2, because in the gas entering the reactor there is certain amount of H_2S as impurity (3.06 mol%, Table 4) and therefore the VGO is already saturated with H_2S at the entrance of the reactor. The maximum concentration of H_2S in the liquid phase is obtained with the countercurrent operation,

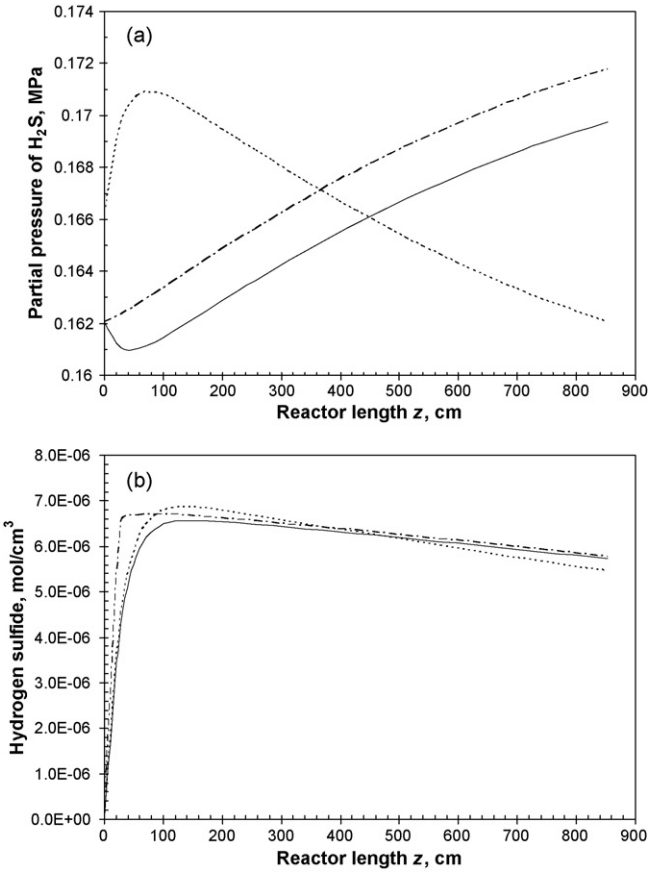

Fig. 8. (a) H_2S partial pressures and (b) concentration profiles at steady state down through the commercial catalytic bed. (▬ · ▬) Cocurrent with H_2 saturated oil, (—) cocurrent with unsaturated oil; (- - -) countercurrent.

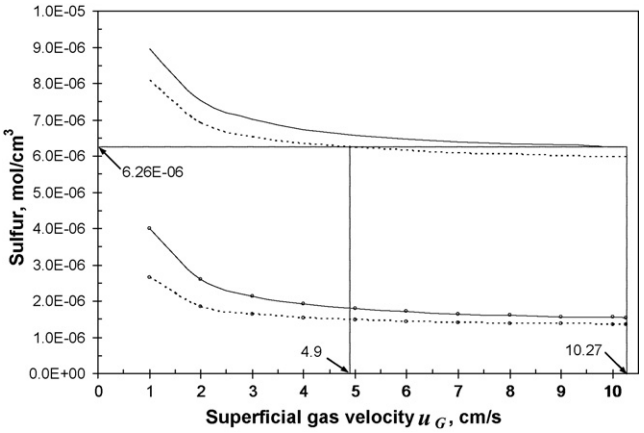

Fig. 9. Effect of superficial gas velocity and H_2S content on product sulfur concentration in commercial reactor. (—) Cocurrent with unsaturated oil and gas feed with 3.06 mol% H_2S content, (- - -) countercurrent with 3.06 mol% H_2S in gas feed, (—⊖—) cocurrent with unsaturated oil and gas feed without H_2S content, (- - ⊖ - -) countercurrent without H_2S in gas feed.

which is due to the higher mass transfer of H_2S from the gas phase to the liquid phase as consequence of the high partial pressure of H_2S at the beginning of the reactor.

It is very important to highlight that in countercurrent operation it is not possible to use the same catalyst particles sizes (1–5 mm) as those employed in cocurrent operation because of flooding [8]. That is why some authors have proposed the use of other types of internals such as "three levels of porosity" packing, monolithic structures or packing of the random type (rings, saddles, etc.). In all the simulations developed in this work it was assumed that properties of the catalyst used in cocurrent operation are equal to those proposed to be employed in countercurrent operation [30].

Since in commercial operations it is possible to obtain higher H_2 purity in the recycle gas stream to the reactor using an amine contactor, a hydrogen purification process (e.g. pressure swing adsorption, or PSA) and/or a source of makeup hydrogen with high H_2 purity (available at about 99.9 mol% H_2 purity), we have then simulated the HDT process by reducing H_2S content from 3.06 to 0 mol% and also varying the superficial velocity (u_G) of the gas phase fed to the commercial HDT unit for cocurrent and countercurrent modes of operation. Fig. 9 shows that sulfur content at the outlet of the reactor decreases as the superficial gas velocity increases for both modes of operation. The superficial gas velocity is directly related to the H_2-to-oil ratio; that is, the value employed in the simulations for the commercial reactor, 10.27 cm/s, corresponds to a H_2/oil ratio of 2000 ft^3/barrel. As depicted by Fig. 9 the countercurrent operation needs a superficial gas velocity of 4.9 cm/s (954 ft^3/barrel H_2/oil ratio) in comparison with 10.27 cm/s of the cocurrent operation in order to reach the same sulfur concentration at the exit of the reactor (6.26×10^{-6} mol/cm^3), which means a reduction of gas flow rate of about 50%. It is important to take into account that although the reduction of gas flow rate or H_2-to-oil ratio yields benefits for countercurrent operation in terms of lower sulfur content in the product, it has certain disadvantages such as [12]:

- Lower dilution of inhibiting compounds (i.e. H_2S, NH_3, etc.) by low H_2 partial pressure.
- Rapid catalyst deactivation.
- Shorter catalyst cycle life by faster coke deposition.
- Increase of the start-of-run temperature.
- Lower throughput capability.
- Higher purge gas flow.
- The HDS rate of refractory sulfur compounds may be limited by a thermodynamically mandated low hydrogenation rate.
- The catalyst surface may be starved of adsorbed hydrogen.

When the gas phase is free of H_2S the conversions of sulfur in the commercial HDT unit obtained with cocurrent and countercurrent modes of operation are 95.5 and 96.1%, respectively, which are higher than those determined when gas phase contained H_2S (81.9 and 82.8%, respectively). When the gas phase is fed to the reactor without H_2S the countercurrent operation needs 39% (61% reduction) of the gas flow rate required by the cocurrent operation in order to obtain the same sulfur concentration at the exit of the reactor (1.54×10^{-6} mol/cm^3), this percentage of gas flow rate reduction was also reported by Yamada and Goto [28] when comparing cocurrent and countercurrent modes of operation in industrial scale.

5. Conclusions

A trickle-bed reactor model was employed in this work to predict the behavior of pilot and commercial hydrotreating reactors in cocurrent and countercurrent modes of operation. The TBR model is one-dimensional plug-flow heterogeneous and includes the most important HDT reactions (HDS, HDN, and HDA). According to all simulations results the following conclusions can be pointed out:

- Countercurrent operation yields lower sulfur and other impurities contents in the product than cocurrent operation even at high liquid velocities as those used in commercial reactors.
- Mass transfer of H_2S from the liquid to the gas phase prevails thus reducing its inhibiting effects on HDT reactions when reactants move further down the bottom of the reactor. This behavior confirmed that interphase mass-transfer resistance is unlikely to be a limiting factor in the development of countercurrent HDT reactors.
- The gas-phase flow in the countercurrent operation involves a cooling effect throughout the reactor therefore energy-balance equation of gas phase must be included when modeling this mode of operation.
- The lowest concentration of H_2S at the bottom of the reactor in countercurrent operation allows it to be improved by using two-stage technologies and grading of more active catalysts although more sensitive to H_2S inhibition.
- The development of novel designs of internals or hardware to improve the overall performance of countercurrent TBR is clearly justified with the modeling results discussed in this work.

Acknowledgment

The authors thank Instituto Mexicano del Petróleo for its financial support.

References

[1] E. Pedernera, R. Reimert, N.L. Nguyen, V. van Buren, Catal. Today 79–80 (2003) 371.
[2] I.I. Rahmin, Oil Gas J. 103 (2005) 18.
[3] T.C. Ho, D. Nguyen, Chem. Eng. Commun. 193 (2006) 460.
[4] W. Wache, L. Datsevich, A. Jess, G. Neumann, Fuel 85 (2006) 1483.
[5] A. Montagna, Y.T. Shah, Chem. Eng. J. 10 (1975) 99.
[6] C.N. Satterfield, AIChE J. 21 (1975) 209.
[7] M.H. Al-Dahhan, F. Larachi, M.P. Dudukovic, A. Laurent, Ind. Eng. Chem. Res. 36 (1997) 3292.
[8] A. Kundu, K.D.P. Nigam, A.M. Duquenne, H. Delmas, Rev. Chem. Eng. 19 (2003) 531.
[9] D.C. McCulloch, Appl. Ind. Catal. 1 (1983) 69.
[10] B.C. Gates, J.R. Katzer, G.C.A. Schuit, Chemistry of Catalytic Processes, third ed., McGraw-Hill, New York, 1979.
[11] T. Kabe, Y. Aoyama, D. Wang, A. Ishihara, W.H. Qian, M. Hosoya, Q. Zhang, App. Catal. A Gen. 209 (2001) 237.
[12] J. Ancheyta, Reactors for hydroprocessing, in: J. Ancheyta, J.G. Speight (Eds.), Hydroprocessing of Heavy Oils and Residue, Taylor & Francis, New York, 2007 (Chapter 5).
[13] P. Trambouze, Chem. Eng. Sci. 45 (1990) 2269.
[14] J.W. Relly, G. Hamilton, US Patent 5, 183 (1993) 556.
[15] J.W. Reilly, M.C. Sze, U. Saranto, U. Schmidt, N. Oy, Oil Gas J. 71 (1973) 66.
[16] K.M. Jackson, Hyd. Proc. 82 (2003) 31.
[17] I.V. Babich, J.A. Moulijn, Fuel 82 (2003) 607.
[18] G.F. Froment, G.A. Depauw, V. Vanrysselberghe, Ind. Eng. Chem. Res. 33 (1994) 2975.
[19] H. Korsten, U. Hoffmann, AIChE J. 42 (1996) 1350.
[20] R. Lopez, C.G. Dassori, SPE 69499 (2001).
[21] M. Bhaskar, G. Valavarasu, A. Meenakshisundaram, K.S. Balaraman, Pet. Sci. Technol. 20 (2002) 251.
[22] R. Chowdhury, E. Pedernera, R. Reimert, AIChE J. 48 (2002) 126.
[23] D.G. Avraam, I.A. Vasalos, Catal. Today 79–80 (2003) 275.
[24] M.A. Rodríguez, J. Ancheyta, Energy Fuels 18 (2004) 789.
[25] F.S. Mederos, M.A. Rodríguez, J. Ancheyta, E. Arce, Energy Fuels 20 (2006) 936.
[26] C. Murali, K.V. Ravi, N. Ravichander, D.T. Gokak, N.V. Choudary, Fuel 86 (2007) 1176.
[27] B.W. van Hasselt, P.J.M. Lebens, H.P.A. Calis, F. Kapteijn, S.T. Sie, J.A. Moulijn, C.M. van den Bleck, Chem. Eng. Sci. 54 (1999) 4791.
[28] H. Yamada, S. Goto, Korean J. Chem. Eng. 21 (2004) 773.
[29] Z. Cheng, X. Fang, R. Zeng, B. Han, L. Huang, W. Yuan, Chem. Eng. Sci. 59 (2004) 5465.
[30] K. Jakobsson, A. Hasanen, J. Aittamaa, Trans. IChemE, Part A, Chem. Eng. Res. Des. 82 (A2) (2004) 203.
[31] J.A. Ojeda, R. Krishna, Trans. IChemE, Part A, Chem. Eng. Res. Des. 82 (2004) 208.
[32] M.P. Dudukovic, F. Larachi, P.L. Mills, Catal. Rev. 44 (2002) 123.
[33] H.P. Hofmann, Catal. Rev.-Sci. Eng. 17 (1978) 71.
[34] R. Krishna, S.T. Sie, Chem. Eng. Sci. 49 (1994) 4029.
[35] S. Goto, J.M. Smith, AIChE J. 24 (1978) 294.
[36] I. Iliuta, F.C. Thyrion, L. Bolle, M. Giot, Chem. Eng. Technol. 20 (1997) 171.
[37] A. Gianetto, V. Specchia, Chem. Eng. Sci. 47 (1992) 3197.
[38] G. Biardi, G. Baldi, Catal. Today 52 (1999) 223.
[39] A. Dietz, C. Julcour, A.M. Wilhelm, H. Delmas, Catal. Today 79–80 (2003) 293.
[40] C.N. Satterfield, Mass Transfer in Heterogeneous Catalysis, MIT Press, Cambridge, Mass., 1970.
[41] A. Bondi, Chem. Tech. 3 (1971) 185.
[42] P.A. Ramachandran, R.V. Chaudhari, Chem. Eng. 87 (1980) 74.
[43] L.K. Doraiswamy, M.M. Sharma, Heterogeneous Reactions: Analysis, Examples, and Reactor Design, vol. 2, John Wiley & Sons, New York, 1984.
[44] T.B. Zhukova, V.N. Pisarenko, V.V. Kafarov, Int. Chem. Eng. 30 (1990) 57.
[45] H. Hofmann, Int. Chem. Eng. 17 (1977) 19.
[46] T. Sutikno, Oil Gas J. 97 (1999) 55.
[47] S. Goto, J.M. Smith, AIChE J. 24 (1978) 286.
[48] Y.T. Shah, G.J. Stiegel, M.M. Sharma, AIChE J. 24 (1978) 369.
[49] S.K. Bej, A.K. Dalai, J. Adjaye, J. Energy Fuels 15 (2001) 377.
[50] S.M. Yui, E.C. Sanford, 1985 Proceedings – Refining Department: 50th Midyear Meeting (Kansas City, MO, May 13–16, 1985), American Petroleum Institute, Washington, DC, 1985, pp. 290–297.
[51] M.O. Tarhan, Catalytic Reactor Design, McGraw-Hill, New York, 1983.
[52] J. Carberry, Chemical and Catalytic Reaction Engineering, McGraw-Hill, New York, 1976.